International Journal of Biochemistry and Cell Biology 115 (2019) 105571

Contents lists available at ScienceDirect

International Journal of Biochemistry and Cell Biology

journal homepage: www.elsevier.com/locate/biocel

Downregulation of microRNA-196a inhibits stem cell self-renewal ability and stemness in non-small-cell lung cancer through upregulating GPX3 expression

Qin Liu[a], Wei Bai[a], Fang Huang[a], Jian Tang[b], Xiang Lin[b,*]

[a] Department of Respiratory and Critical Care Medicine, The First Affiliated Hospital of Nanchang University, Nanchang 330006, PR China
[b] Department of Thoracic Surgery, The First Affiliated Hospital of Nanchang University, Nanchang 330006, PR China

ARTICLE INFO

Keywords:
microRNA-196a
Non-small-cell lung cancer
GPX3
JNK pathway
Self-renewal ability
Stemness

ABSTRACT

Studies have reported a high expression profile of microRNA-196a (miR-196a) in many cancers, which potently plays important roles in carcinogenesis. However, the involvement of miR-196a in affecting non-small cell lung cancer (NSCLC) carcinogenesis still remains uncertain. NSCLC-related differentially expressed genes were retrieved for this study according to the microarray-based analysis, which demonstrated that miR-196a may be involved in NSCLC progression *via* regulation of the Jun **N**-terminal kinase (JNK) pathway by targeting glutathione peroxidase 3 (GPX3). Hence, this study aimed to explore the relationship among miR-196a, GPX3, and the JNK pathway and to investigate its functional regulations in NSCLC. Initially, highly-expressed miR-196a and lowly-expressed GPX3 were determined in NSCLC tissues and cells. Next, the NSCLC cells were manipulated with a series of mimic, inhibitor or shRNA to investigate the impact of miR-196a and GPX3 on CSC viability, proliferation, self-renewal ability and stemness. The *in vivo* effect of miR-196a was measured in nude mice xenografted with NSCLC cells. The results demonstrated that downregulation of miR-196a and restoration of GPX3 inhibited CSC viability, proliferation, self-renewal ability, stemness and tumorigenicity. Meanwhile, the underlying relationship among miR-196a, GPX3 and JNK pathway was explored by treatment with the JNK pathway inhibitor (SP600125), or sh-GPX3. Downregulated miR-196a and upregulated GPX3 could elevate the GPX3 protein expression and reduce the extent of JNK and c-Jun phosphorylation. Taken together, miR-196a promotes the development of NSCLC *via* activation of the JNK pathway through down-regulation of GPX3 and serve as a potential therapeutic target in NSCLC.

1. Introduction

Lung cancer represents one of the most universal malignant tumors among human beings, particularly non-small cell lung cancer (NSCLC), accompanied by high mortality and frequent recidivation worldwide (Xu et al., 2018). NSCLC accounts for over 80% of lung cancer with squamous cell carcinoma and adenocarcinoma as its main forms, which might be induced by cigarette smoking, as well as carcinogens and hereditary factors (Apopa et al., 2018). Currently, various therapeutic methods have been practiced in the clinical setting for NSCLC management, with surgical intervention still persisting as the standard treatment option, but only 30% of NSCLC patients meeting the conditions of curative resection (Mauguen et al., 2013). Besides, radical thoracic radiotherapy was practiced in patients with locally advanced NSCLC, with or without chemotherapy; and palliative treatments for patients at an advanced stage (Yang et al., 2018). Although with the aforementioned therapeutic methods, NSCLC patients still face unsatisfactory 5-year overall survival rate of around 15% and a high recurrence rate (Jin et al., 2018; Yin et al., 2018). Therefore, it is urgent to seek out other potential therapeutic approaches for NSCLC treatment.

Glutathione peroxidase 3 (GPX3) is known as a modulator of redox

Abbreviations: NSCLC, Non-small-cell lung cancer; CSC, Cancer stem cells; GPX3, Glutathione peroxidase 3; GEO, Gene Expression Omnibus; DEGs, Differentially expressed genes; PPI, Protein-protein interaction; ATCC, American Type Culture Collection; RPMI, Roswell Park Memorial Institute; HBECs, Human bronchial epithelial cell line; FBS, Fetal bovine serum; 3'UTR, 3'untranslated region; DMSO, Dimethylsulfoxide; PBSDNTPs, Phosphate buffer saline; ALDH1, Aldehyde dehydrogenase 1

* Corresponding author at: Department of Thoracic Surgery, The First Affiliated Hospital of Nanchang University, No. 17, Yongwai Street, Nanchang 330006, Jiangxi Province, PR China.
E-mail address: lxlinxiang2018@126.com (X. Lin).

https://doi.org/10.1016/j.biocel.2019.105571
Received 14 January 2019; Received in revised form 2 July 2019; Accepted 16 July 2019
Available online 25 July 2019
1357-2725/

signaling and an antioxidant enzyme, which can achieve immunomodulatory regulation and accelerate reactive oxygen species detoxification (An et al., 2016). A recent study has reported that GPX3 exerts a suppressive effect on lung cancer cell proliferation through modulation of the redox-regulated signals (An et al., 2018). Moreover, a higher expression profile of GPX3 has been demonstrated to be associated with better overall survival in patients with NSCLC (Liu et al., 2018). According to online prediction software and dual luciferase reporter gene assay, GPX3 was ascertained as a target of microRNA-196a (miR-196a). An existing report emphasized on the relevance of up-regulation of miR-196a in NSCLC cells, and potentiated it to function as an oncogenic miR to promote cell proliferation and invasion *via* down-regulation of homeobox A5 (Liu et al., 2012). Besides, the down-regulation of miR-196a was indicated to sensitize NSCLC cells to cisplatin treatment for better therapeutic results (Li et al., 2016). JNK, a protein kinase, can be activated by a variety of stress stimuli such as DNA damage, shear stress, inflammatory cytokines, heat shock and oxidative stress (Avisetti et al., 2014). The JNK pathway has been illustrated to be associated with NSCLC cell proliferation and invasion through diversion (Luan et al., 2014). In oral cancer, miR-196 enhanced cell migration and invasion due to the involvement of an increased content in JNK phosphorylation (Lu et al., 2014). With the aforementioned literature, it can be hypothesized that miR-196a may affect the biological characteristics of NSCLC stem cells through regulation of GPX3 and the JNK pathway. Therefore, this study was performed to testify this hypothesis and offer a better understanding of the underlying molecular mechanisms responsible for NSCLC progression, thus providing an insight for more effective therapeutic strategies for NSCLC patients.

2. Materials and methods

2.1. Ethics statement

This study was conducted under the approval of the Ethics Committee of The First Affiliated Hospital of Nanchang University. All participating patients signed written informed consent documentation prior to enrollment. Mice were treated humanely, and all experimental procedures were performed under the approval of the Institutional Animal Care and Use Committee. Measures were taken to minimize animal suffering.

2.2. Microarray-based analysis

The NSCLC-related gene expression chips (GSE101929, GSE103512, GSE19188, and GSE33532), as displayed in Table 1, were retrieved from the Gene Expression Omnibus (GEO) database (https://www.ncbi.nlm.nih.gov/geo/) to screen for the differentially expressed genes (DEGs). The Affy package (Gautier et al., 2004) of R language was employed for both pre-processing and standardization of the gene expression data, and the limma package (Smyth, 2004) was adopted for a cycle of DEGs screening between the NSCLC tissues and normal tissues (*adj.p.Val* referred to a corrected *p* value). The screening threshold for DEGs was set as $|\text{LogFoldChange}| > 2$ and $adj.p.Val < 0.05$, and the DEG expression thermal maps were drawn in reference to the values. Next, comparison of DEGs in four chips was conducted from the gene intersection obtained by using calculate and draw custom Venn diagrams (http://bioinformatics.psb.ugent.be/webtools/Venn/). The disease-gene association (Kim et al., 2013) was ascertained by searching for MEDLINE abstracts in the DiGSeE disease gene search engine (http://210.107.182.61/geneSearch/), from which genes relevant to NSCLC were retrieved. According to the protein-protein interaction (PPI) information provided by the String database (https://string-db.org/) (Szklarczyk et al., 2015), Cytoscape 3.6.0 software (Shannon et al., 2003) was employed to extract the PPI network constructed by DEGs in NSCLC and disease genes, furthermore to select vital molecules in NSCLC. Ultimately, the potential miRs speculated to regulate DEGs were predicted by TargetScan (http://www.targetscan.org/vert_71/), miRDB (http://www.mirdb.org/) and miRDIP (http://ophid.utoronto.ca/miRDIP/), and the prediction results were compared using calculate and draw custom Venn diagrams.

2.3. Study subjects

Human NSCLC cell lines A549, H460, H1975, H1650 and HCC827 were purchased from the American Type Culture Collection (ATCC, Manassas, VA, USA). The normal human bronchial epithelial cell line (HBECs) (Shanghai Maisha Biotechnology, Shanghai, China) was subjected to culture in Roswell Park Memorial Institute (RPMI) 1640 medium containing a combination of 10% fetal bovine serum (FBS), 100 U/mL penicillin and 100 mg/L streptomycin in a 5% CO_2 incubator at 37 °C. Subsequently, the cells were treated with 0.25% trypsin and passaged. The cells in the logarithmic growth phase were obtained for further experimentation.

A total of 80 NSCLC samples were collected from patients with NSCLC, comprising of 45 males and 35 females, who underwent radical resection in the Department of Thoracic Surgery of The First Affiliated Hospital of Nanchang University between January 2016 and January 2017. The tumor tissues and the normal adjacent tissues were obtained from each case. The inclusion criteria for selection of patients were as follows: patients diagnosed with NSCLC with an intention to undergo surgery; patients who underwent radical resection and presented with postoperative pathology characteristic of tumor-free margins; patients with complete clinical related and pathological examination; patients who had not received any anti-tumor-related treatment without heart, liver and renal insufficiency, and without any serious respiratory diseases. The patients diagnosed with metastatic lung cancer and other tumors, cardio-cerebrovascular diseases, infectious diseases, history of alcohol abuse and mental illness were excluded from this study.

2.4. Cell counting kit (CCK-8) assay

The proliferation of NSCLC CSCs was detected using a CCK-8 assay kit (CK04, Dojindo, JPN, Kumamoto, Japan). CSCs were trypsinized, inoculated into a 96-well plate and cultured at 37 °C in 5% CO_2 until the cells adhering to the wall. The cell concentration was adjusted to 5000 cells/well, 6 repeated wells for each group. The cells were cultured at 37 °C in 5% CO_2 and the plate was removed after transfection for 24, 48, 72 and 96 h, followed by the addition of 10% CCK-8 solution, and subsequent incubation for 4 h. The optical density (OD) was detected at

Table 1
Detailed information for NSCLC related-gene expression chips.

Accession	Platform	Organism	Sample
GSE101929	GPL570	Homo sapiens	34 normal lung tissues and 32 NSCLC tumor
GSE103512	GPL13158	Homo sapiens	60 NSCLC samples and 9 normal samples
GSE19188	GPL570	Homo sapiens	91 NSCLC tumor and 65 normal adjacent lung tissue samples
GSE33532	GPL570	Homo sapiens	80 NSCLC primary tumors and 20 distant normal lung tissues

Note: NSCLC, non-small-cell lung cancer.

an excitation wavelength of 450 nm using a microplate reader, from which the cell growth curve was drawn (Cao et al., 2018). The experiment was conducted three times independently.

2.5. Dual-luciferase reporter gene assay

The cloning of -881/+1546 region of GPX3 3′untranslated region (3′UTR) was performed with cDNA of A549 cells as a template. The target-binding site between miR-196a and the GPX3 gene was predicted by means of bioinformatics analysis, and site-directed mutant was performed on the binding site. The 3′UTR-wild type (WT) vector was used as a template to construct the GPX3 3′UTR-mutant (MUT) reporter vector using the QuikChange Site-Directed Mutagenesis kit (Stratagene, La Jolla, CA, USA), where the GPX3 3′UTR site sequence CAGUUCUC upon recognition by miR-196a was mutated to GTAAGAG. The primer sequences for GPX3 3′UTR amplification (-881 [SacI], 5′-gagctcc-tattctcaaaggactcctggt-3′, +1546 [HindIII] and 5′-aagcttttc-caatgggcttcctgag-3′) were then recombined into the pmiR-REPORT miR vector (Ambion, Austin, Texas, USA) and transfected with *Escherichia coli* DH5α in order to amplify recombinant plasmid vector amplification. The pRL-TK vector expressing renilla luciferase was employed as an internal reference to adjust the difference in cell number and transfection efficiency. Next, miR-196a mimic, miR-196a mimic-negative control (NC), miR-196a inhibitors, miR-196a inhibitor-NC (4464084, ABI, Oyster Bay, NY, USA) were co-transfected with the dual-luciferase reporter vectors into Hela cells, respectively. The detection of dual-luciferase activity was performed in strict accordance with the instructions provided by the Promega Corporation (Madison, WI, USA). The experiments were conducted 3 times independently.

2.6. Sorting of NSCLC cells and cell cycle detection

The NSCLC cells in logarithmic growth phase were rinsed twice using phosphate buffer saline (PBS), and adjusted to a concentration of 1×10^7 cells/mL. Antibodies against CD133-PE (566593, 1 : 500) and CD44-FITC (555478, 1 : 500) were added to the cells for incubation at room temperature for 30 min and then rinsed twice with PBS. The aforementioned antibodies were purchased from BD Biosciences (Franklin Lakes, NJ, USA). Next, the cells were suspended using 1 mL PBS, filtered through a 40-μm sterile mesh and positioned on ice for further analysis and sorting. Isotype control antibody cell group was labeled under similar conditions. The NSCLC cells prepared for further analysis were sorted using a FACSAria II flow cytometer (BD Biosciences, Franklin Lakes, NJ, USA). After the cell samples were placed on the flow cytometer, the CD133 and CD44 double positive cells were sorted according to the fluorescent labeling characteristics of different antibodies. Finally, the sorted cells were aseptically collected into sorting tubes.

After transfection for 48 h, the NSCLC cells were collected and rinsed using cold PBS 3 times. Then, the cells were centrifuged and the supernatant was removed. The cell concentration was adjusted to about 1×10^5 cells/mL, the NSCLC cells were fixed utilizing 1 mL 75% cold ethanol overnight at 4 °C. Before staining, the cells were rinsed two times with the supernatant removed, added with 100 μL of RNase A devoid of light, and water-bathed at 37 °C for 30 min. The NSCLC cells were stained with 400 μL propidium iodide (PI) (Sigma-Aldrich, St Louis, MO, USA), in conditions devoid of light at 4 °C for 30 min. The flow cytometry (FACS-Canto II, BD Biosciences, Franklin Lakes, NJ, USA) was used to record the red fluorescence at a wavelength of 480 nm to detect the cell cycle (Halim et al., 2016).

2.7. Cell grouping and transfection

NSCLC cells in the logarithmic growth phase were seeded into 6-well plates (6–7 × 10^5 cells/well), and cell transfection was conducted in strict accordance with the instructions of the Lipofectamine 2000 transfection kit. Each well was added with 25 pmol corresponding plasmids and 10 μL transfection reagent with the final concentration reaching 10 pmol/mL by gentle shaking. Then, the plates were subjected to culture at 37 °C and with 5% CO_2 for 48 h.

Next, the cells were grouped into 12 groups: miR-196a mimic (cells transfected with synthetic miR-196a mimic), miR-196a mimic-NC (cells transfected with miR-196a mimic nonsense sequences), miR-196a inhibitor (cells transfection with miR-196a inhibitor), miR-196a inhibitor-NC (cells transfected with miR-196a inhibitor nonsense sequences), sh-GPX3 (cells transfected with sh-GPX3), sh-GPX3 NC (cells transfected with empty plasmid vector), SP600125 (cells treated with JNK pathway inhibitor), dimethylsulfoxide (DMSO) (cells treated with DMSO, control of SP600125 group), miR-196a inhibitor + sh-GPX3 (cells co-transfected with miR-196a inhibitor and sh-GPX3), miR-196a inhibitor + sh-GPX3 NC (cells co-transfected with miR-196a inhibitor and empty plasmid vector), miR-196a mimic + SP600125 (cells treated with synthetic miR-196a mimic and JNK pathway inhibitor) and miR-196a mimic + DMSO (cells treated with synthetic miR-196a mimic and DMSO) groups. The experiments were repeated 3 times independently.

2.8. Reverse transcription quantitative polymerase chain reaction (RT-qPCR)

The Trizol kit (16096020, Thermo Fisher Scientific, Massachusetts, CA, USA) was employed to extract the total RNA from the specimens. Then, 5 μg RNA was reversely transcribed into cDNA using the RT-qPCR kit (ABI Company, Oyster Bay, N.Y., USA), while the miR reverse transcription and PCR quantification were conducted using the miScript II RT kit (218161, QIAGEN GmbH, Hilden, Germany) and the miScript SYBR®GreenPCR kit (218075, QIAGEN GmbH, Hilden, Germany). A 25 μL system was employed for PCR amplification, which was comprised of 300 ng cDNA, 1 × PCR buffer, 200 μmol/L deoxyribonucleoside triphosphates (dNTPs), 80 pmol/L forward primers, 80 pmol/L reverse primers and 0.5 U Taq enzyme (S10118, Shanghai Yuanye Biotechnology Co., Ltd., Shanghai, China). The reaction conditions were as follows: predenaturation at 94 °C for 5 min, 30 cycles of denaturation at 94 °C for 30 s, annealing at 54.5 °C for 30 s and extension at 72 °C for 30 s, and extension at 72 °C for 10 min, respectively. The obtained PCR amplification products were stored at 4 °C. The primer sequences of miR-196a, U6, GPX3, β-actin, NSCLC surface markers (CD133 and CD44), and related transcription factors sex-determining region Y-box 2 (SOX2), octamer-binding transcription factor 4 (OCT4) and aldehyde dehydrogenase 1 (ALDH1) are presented in Table 2. U6 was regarded as the internal reference for the relative miR-196a expression profile, and β-actin was employed as the internal reference for the relative expression of other genes. $2^{-\Delta\Delta Ct}$ method was adopted in order to calculate the ratio of the relative gene expression in the experimental group to that in the control group with the following formula: $\triangle\triangle Ct = \triangle Ct_{\text{the experimental group}} - \triangle Ct_{\text{the control group}}$, and $\triangle Ct = Ct_{\text{(target gene)}} - Ct_{\text{(internal reference)}}$. Ct referred to the amplification cycles when the real-time fluorescence intensity reached the set threshold value and the amplification entered a logarithmic growth. The experiments were repeated 3 times independently.

2.9. Western blot analysis

The NSCLC tissues or cells of each group were rinsed twice with PBS, added with cell lysis buffer and shaken with vortex. The cells were centrifuged at 25,762 × g for 30 min to remove the tissue or cell debris, with the supernatant obtained. Next, the total protein concentration was determined using a bicinchoninic acid (BCA) assay kit. A total of 50 μg protein was dissolved in 2 × sodium dodecyl sulfate (SDS) loading buffer and boiled at 100 °C for 5 min. Next, the samples were separated using 10% sodium dodecyl sulfate-polyacrylamide gel electrophoresis (SDS-PAGE), transferred onto the polyvinylidene fluoride (PVDF) membrane by wet transfer method, and blocked using 5% skim

Table 2
Primer sequences for RT-qPCR.

Primers	Forward	Reverse	Temp	Length
miR-196a	5' -CGTCAGAAGGAATGATGCACAG -3'	5' -ACCTGCGTAGGTAGTTTCATGT -3'	52	–
U6	5' -CGCAAGGATGACACGCAAAT -3'	5' –GTATATGTGCTGCCGAAGCGAGCAC- 3'	55	69
GPX3	5' -TGGTCATTCTGGGCTTTCCC- 3'	5' -CCAGAAGAGGCGGTCAGATG-3'	56	233
β-actin	5' -CTTCCAGCCTTCCTTCCTGG- 3'	5' -CTGTGTTGGCGTACAGGTCT-3'	58	110
CD133	5' -AACAGTTTGCCCCCAAGGAAA- 3'	5' -GAAGGACTCGTTGCTGGTGA-3'	54	85
CD44	5' -CACACCCTCCCCTCATTCAC- 3'	5' -TTGGCGATATCCCTCATGCC-3'	55	155
SOX2	5' -AACCAGCGCATGGACAGTTA- 3'	5' -CGAGCTGGTCATGGAGTTGT-3'	56	180
OCT4	5' -GAAGCCTTTCCCCCTGTCTC- 3'	5' -AAACCCTGGCACAAACTCCA-3'	54	137
ALDH1	5' -AGGGGCAGCCATTTCTTCTC- 3'	5' -ATGCAAGGGCTCTTTCCTCC-3'	56	144
E-cadherin	5' -ACAACGCCCCCATACCAGA- 3'	5' -CACTCGCCCCGTGTGTTAGT-3'	54	138
N-cadherin	5' –ATCCTACTGGACGGTTCG- 3'	5' –AGTTGACTGAGGCGGGTG- 3'	54	167

Note: RT-qPCR, reverse transcription quantitative polymerase chain reaction; miR-146, microRNA-196a; GPX3, glutathione peroxidase 3; ALDH1, aldehyde dehydrogenase 1; SOX2, sex-determining region Y-box 2; OCT4, octamer-binding transcription factor 4; ALDH1, aldehyde dehydrogenase 1; Temp, temperature.

milk for 1 h at room temperature. Then, the membrane was subjected to incubation after the addition of the following diluted primary antibodies against β-actin (ab8226, 1 : 1000), GPX3 (ab104448, 1 : 5000), JNK (ab179461, 1 : 500), p-JNK (ab219584, 1 : 1000), c-Jun (ab32137, 1 : 500), p-c-Jun (ab32385, 1 : 1000), CD133 (ab19898, 1 : 3000), CD44 (ab51037, 1 : 250), SOX2 (ab97959, 1 : 500), homeobox protein NANOG (NANOG) (ab21624, 1 : 500), OCT4 (ab181557, 1 : 2000), ALDH1 (ab23375, 1 : 2000), monoclonal antibody against rabbit E-cadherin (ab40772, 1 : 10,000) and polyclonal antibody against rabbit N-cadherin (ab76057, 1 : 1000). The aforementioned antibodies were purchased from Abcam (Shanghai, China). Afterwards, the membrane was rinsed 3 times using tris buffered saline with tween (TBST), followed by incubation with the horseradish peroxidase (HRP)-labeled secondary antibody for 1 h. Next, the membrane was rinsed with TBST and placed on a clean glass plate. Subsequently, solution A and solution B in the enhanced chemiluminescence (ECL) kit (BB-3501, GE Healthcare, Piscataway, NJ, USA) were mixed in an equal volume under conditions devoid of light, which was then added into the membrane. Bio-Rad image analysis system (Bio-Rad Laboratories, Hercules, CA, USA) was used to photograph and document the observations, and the Quantity One v4.6.2 software was utilized for analysis. At last, the relative protein levels were expressed as the ratio of the gray value of the target protein bands to the β-actin protein band. The experiments were repeated 3 times independently.

2.10. Oncospheroids formation assay

After cells in the logarithmic growth phase were treated with 0.125% trypsin, the trypsin was neutralized by the addition of medium with serum. The detached cells were centrifuged and the supernatant was discarded, and resuspended in the medium, followed by inoculation into the 96-well plate pretreated with agarose at a low melting point and incubation in a CO_2 incubator at 37 °C. After 7 days, the cells developed into tumor spheres with a volume of approximately 0.5 mm^3. The radius of the tumor sphere was observed using the eyepiece with a ruler, and the volume of the tumor sphere was calculated using the spherical volume formula: $V = (4/3)\ \pi R^3$. Any change in tumor volume size was recorded and analyzed.

2.11. Colony formation assay

The 0.7% agarose with a low melting point was prepared using the fresh cell culture medium and stored at 4 °C for further use. When agar had settled, 0.7% agarose was heated and thawed, 2 mL of which was evenly spread on the bottom of a culture dish with a diameter of 100 mm by gently shaking, cooled and solidified. Next, 1 mL cell suspension was diluted with an equal volume of 0.7% agarose to prepare 0.35% agarose cell mixed liquor, which was then seeded into the culture dish (1×10^4 cells per 100 cm^2). Three parallels were set for each group. After the agar on the upper layer was solidified, 2 ~ 3 mL culture solution was gently added onto its surface (pay attention not to crumble the agar during this process) and incubated at 37 °C with 5% CO_2. The culture medium was changed every 2 ~ 3 day, and the culture was terminated after a month. The culture dish underwent observation under an inverted microscope to count the cells (only a cluster of more than 50 cells was visible as a cell colony), and photographs. The experiments were repeated 3 times independently.

2.12. Xenograft tumor in nude mice

The NSCLC cells in the logarithmic growth phase with a stable transfection status were detached, and adjusted to attain a concentration of 5×10^7 cells/mL using a cytometer. After centrifugation, the cells were mixed in serum-free medium and Matrigel (1 : 1) according to the required amount, and stored at 4 °C. The NOD/SCID immunodeficient male mice (aged 5 ~ 7 weeks, Beijing Vital River Experimental Animal Technology Co. Ltd, Beijing, China; License number: SYXK [Beijing] 2017-0022) were randomly assigned into 8 groups with 7 mice in each group: the miR-196a mimic group, the miR-196a mimic-NC group, the miR-196a inhibitor group, the miR-196a inhibitor-NC group, the sh-GPX3 group, the sh-GPX3-NC group, the miR-196a inhibitor + sh-GPX3 group and the miR-196a inhibitor + sh-GPX3-NC group. The mice were subcutaneously injected with 50 μL of the experimental cell suspension into the left abdominal wall and with 50 μL of control cell suspension into the right abdominal wall using an l mL syringe. The activity and eating habits of mice were observed and documented every day. After 7 ~ 9 weeks, the mice were routinely euthanized to extract the tumor. At last, the tumor was weighed and the tumor volume was analyzed, and photographed.

2.13. Statistical analysis

All statistical analyses were performed using the SPSS 21.0 software (IBM Corp., Armonk, NY, USA). All experimental data was examined for normal distribution and homogeneity of variance. The data consistent with normal distribution were expressed as mean ± standard deviation; while those inconsistent with normal distribution or homogeneity of variance were presented as interquartile range. Pairwise comparison was performed by *t*-test and processed with the post-hoc test. The data with skew distribution were analyzed by the nonparametric Wilcoxon signed rank test. Comparisons between multiple groups were assessed using one-way analysis of variance (ANOVA), and data at different time points were analyzed by repeated ANOVA. A value of $p < 0.05$ was considered to be of statistical significance.

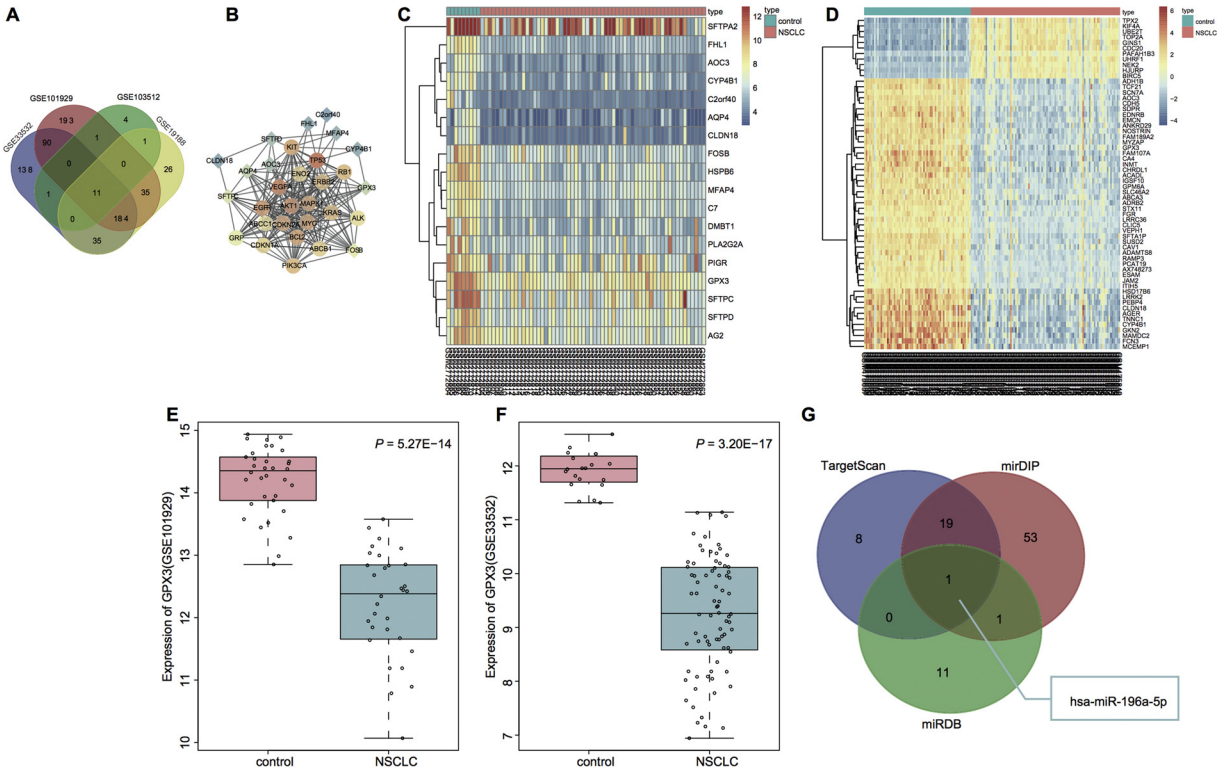

Fig. 1. The miR-196a plays role in NSCLC by regulating the GPX3-mediated JNK pathway in NSCLC. A, 11 intersection DEGs among NSCLC-related gene expression chips (GSE101929, GSE103512, GSE19188, and GSE33532); B, a PPI network of DEGs and disease genes; rhombus indicated the DEGs and circle indicated the disease genes; C and D, thermal maps of the top 60 DEGs screened from GSE103512 and GSE19188 chips, respectively; the horizontal coordinate represented the sample number, and the vertical coordinate represented the DEGs; the upper right histogram was the color gradation in which each rectangle corresponded to one gene expression in one sample; E and F, the expression of GPX3 in the GSE101929 and GSE33532 chips respectively; G, the comparison among predicted miRs obtained from three prediction websites (TargetScan, miRDB and miRDIP); miR-196a, microRNA-196a; GPX3, glutathione peroxidase 3; JNK, Jun NH-terminal kinase; NSCLC, non-small-cell lung cancer; DEGs, differentially expressed genes; PPI, protein-protein interaction.

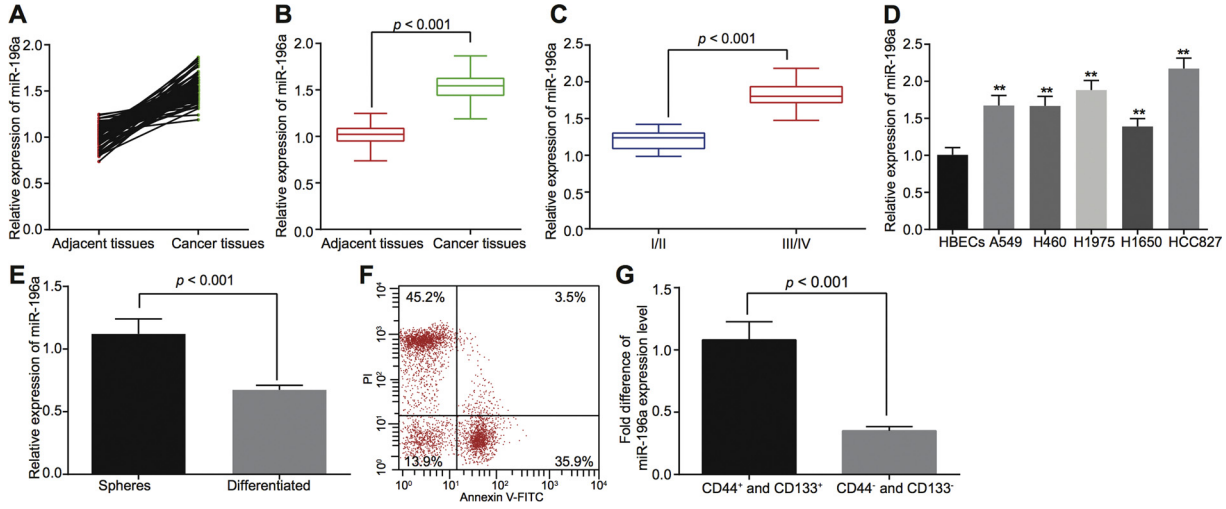

Fig. 2. miR-196a is expressed at a high level in NSCLC cells and tissues. A and B, the expression of miR-196a in cancer tissues and normal adjacent tissues; the horizontal line represented the median of each group; C, miR-196a expression in different clinical stage of NSCLC; D, the expression of miR-196a in NSCLC cell lines (A549, H460, H1975, H1650 and HCC827) and normal bronchial epithelial cell line HBECs; $^{**}p < 0.001$ *vs.* the HBECs; E, the expression of miR-196a in NSCLC A549 cell spheres and differentiated cells; F, the $CD133^+$ and $CD44^+$ cells isolated from A549 cells by flow cytometry; G, the expression of miR-196a in and $CD44^{+/}$ $_{CD44+\ and\ CD133+}$、$_{CD44\ -\ and\ CD133\ -}$ A549 cells; the above data were measurement data and expressed as mean ± standard deviation; comparison between two groups was analyzed by the independent *t*-test, and comparison among multiple groups was performed with one-way analysis of variance; the experiments were repeated 3 times; miR-196a, microRNA-196a; NSCLC, non-small-cell lung cancer; HBECs, human bronchial epithelial cells; +, positive; -, negative.

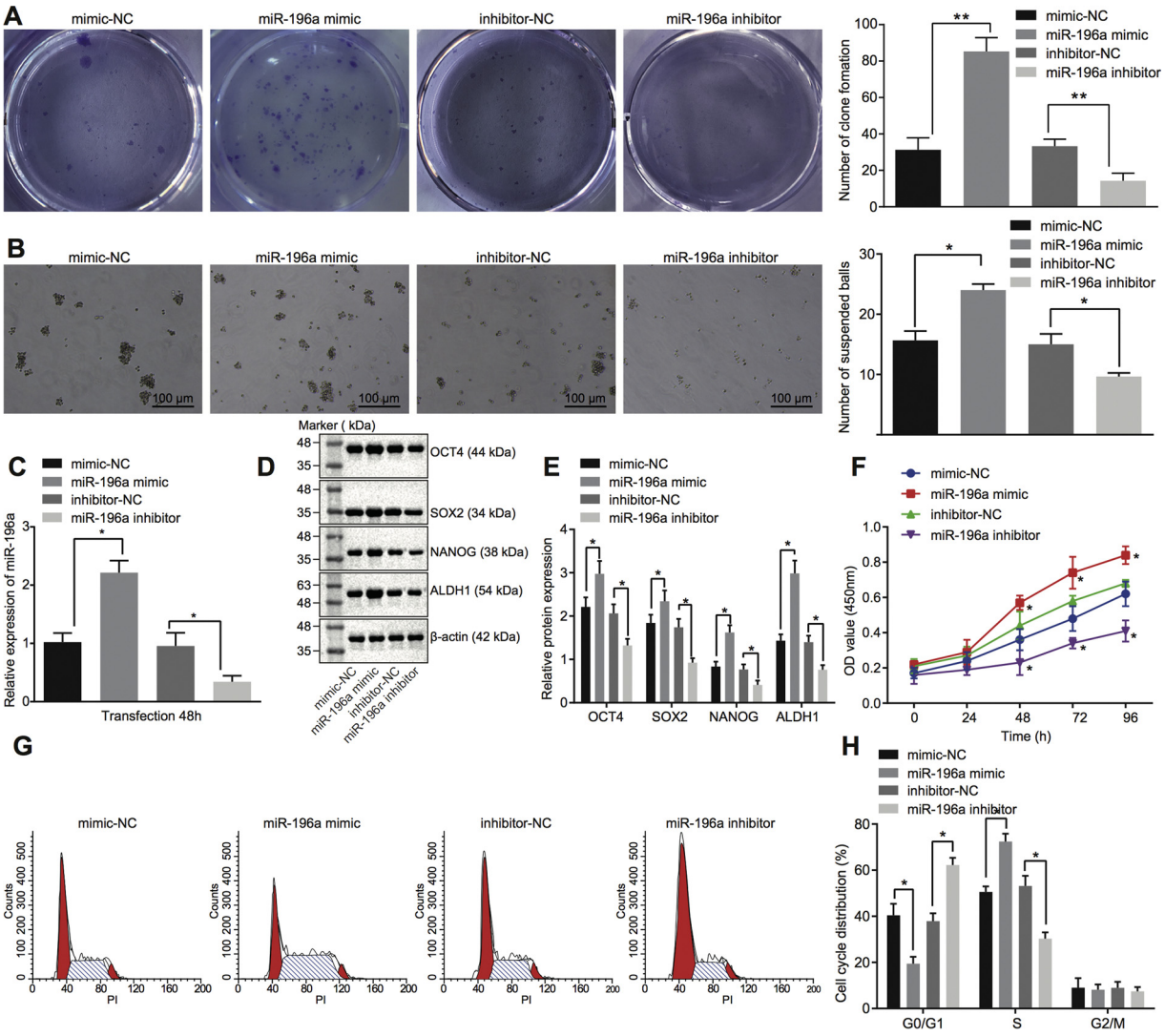

Fig. 3. NSCLC stem cell self-renewal ability and stemness are attenuated upon inhibition of miR-196a. A, cell colony formation ability of NSCLC cells after alteration of miR-196a; B, cell sphere formation ability of NSCLC cells after alteration of miR-196a (× 100); C, miR-196a expression after transfection detected by RT-qPCR; D and E, the relative protein levels of OCT4, SOX2, NANOG and ALDH1 in NSCLC cells after alteration of miR-196a detected by western blot analysis; F, proliferation of NSCLC stem cells after alteration of miR-196a detected by CCK-8 assay; G and H, cell cycle and distribution of NSCLC stem cells after alteration of miR-196a detected by flow cytometry. $^{*}p < 0.05$; the above data were measurement data, expressed as mean ± standard deviation, and analyzed by one-way analysis of variance; the experiments were repeated 3 times; miR-196a, microRNA-196a; NSCLC, non-small-cell lung cancer; ALDH1, aldehyde dehydrogenase 1; NC, negative control; SOX2, sex-determining region Y-box 2; OCT4, octamer-binding transcription factor 4.

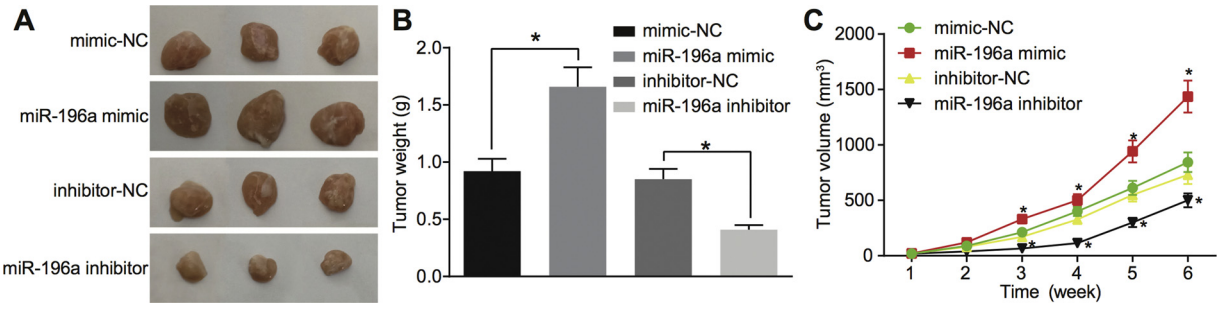

Fig. 4. Tumorigenesis and tumor growth of NSCLC stem cells are suppressed by repressing miR-196a. A, NSCLC tumor growth status in mice after alteration of miR-196a; B, tumor weight in mice after alteration of miR-196a; C, tumor volume at different time points after alteration of miR-196a; $^{*}p < 0.05$; the above data was measurement data and expressed as mean ± standard deviation; comparison among multiple groups were performed with one-way analysis of variance; n = 7; miR-196a, microRNA-196a; NSCLC, non-small-cell lung cancer; NC, negative control.

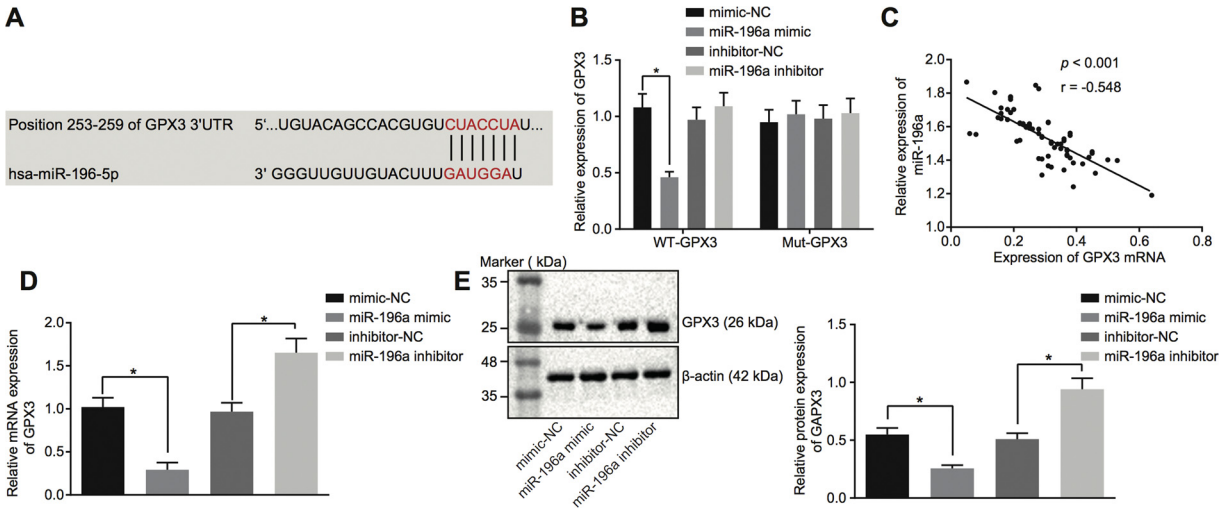

Fig. 5. GPX3 is negatively regulated by miR-196a. A, the predicted binding site between miR-196a and GPX3; B, the targeting relationship between miR-196a and GPX3 as verified by dual-luciferase reporter gene assay; C, the association between miR-196a expression and GPX3 level; D, the GPX3 mRNA level in NSCLC cells after alteration of miR-196a; E, the GPX3 protein level in NSCLC cells after alteration of miR-196a; $^{*}p < 0.05$; the above data were measurement data and expressed as mean ± standard deviation; comparison among multiple groups were performed with one-way analysis of variance; the experiments were repeated 3 times; miR-196a, microRNA-196a; GPX3, glutathione peroxidase 3; NSCLC, non-small-cell lung cancer; NC, negative control; RT-qPCR, reverse transcription quantitative polymerase chain reaction.

3. Results

3.1. miR-196a is speculated to regulate GPX3-mediated JNK pathway in NSCLC

Initially, the R language was employed to screen DEGs from the NSCLC-related gene expression chips. According to the screening threshold of |LogFoldChange| > 2 and *adj.p.Val* < 0.05, a total of 514, 17, 292 and 459 genes were screened from GSE101929, GSE103512, GSE19188 and GSE33532, respectively. Next, a Venn diagram was drawn by comparing the DEGs among these four chips. As depicted in Fig. 1A, 11 intersection genes (MFAP4, AQP4, FHL1, AOC3, SFTPC, SFTPD, GPX3, FOSB, CLDN18, C2orf40, and CYP4B1) were selected for subsequent analysis as NSCLC-related DEGs. The NSCLC disease-related genes were retrieved from DiGSeE, and the first 20 genes (EGFR, TP53, SCLC1, ALK, AKT1, VEGFA, GRP, BCL2, KIT, KRAS, ABCB1, CDKN2A, MYC, ENO2, MAPK1, ERBB2, ABCC1, PIK3CA, CDKN1A, and RB1) were regarded as disease-related genes. Then, a PPI network of the NSCLC-related DEGs and disease-related genes was constructed (Fig. 1B). The genes localized in the center of the PPI network indicated a strong association with other genes and might be of great importance for the disease. The DEG, GPX3 exhibited the strongest correlation with other genes. Subsequently, thermal maps of the top 60 DEGs in GSE103512 and GSE19188 chips were drawn, as respectively displayed in Fig. 1C and 1D. GPX3 was observed to be poorly expressed in NSCLC tissues compared to the normal tissues. The expression of GPX3 in GSE101929 and GSE33532 is respectively shown in Fig. 1E and Fig. 1F, which suggested that the GPX3 expression was poor in NSCLC tissues. Activation of the JNK pathway was previously demonstrated to be associated with NSCLC progression (Song et al., 2014). Moreover, a recent study reported that GPX3 could successfully inhibit JNK signaling (Qi et al., 2016). Therefore, we inferred that GPX3 might impact the progression of NSCLC *via* the JNK pathway. The regulatory miRs of GPX3 were predicted using the TargetScan, miRDB, and miRDIP prediction websites, among which 28, 74 and 13 miRs were with a probability of conserved targeting, integrated Score > 0.2, and Target Score > 80, respectively. Comparison among the prediction results revealed that hsa-miR-196a-5p was the miR in the miR-miR intersection (Fig. 1G), suggesting that miR-196a could potentially regulate GPX3. Moreover, miR-196a was previously demonstrated to express at a high level in NSCLC (Guerriero et al., 2017). The aforementioned results served as basis for the speculation that miR-196a was highly possible to affect the JNK pathway by regulating GPX3 expression in NSCLC.

3.2. miR-196a is upregulated in NSCLC tissues and cells

RT-qPCR was conducted to study the expression of miR-196a in 80 cases of NSCLC and normal adjacent tissues. As depicted in Fig. 2A and B, miR-196a was highly expressed in NSCLC tissues compared to the normal adjacent tissues, with a median difference of about two folds ($p < 0.01$) between these two groups.

Besides, to ascertain the relationship between the expression level of miR-196a and the clinical stage of NSCLC, we detected the miR-196a expression in different clinical stages of NSCLC. As shown in Fig. 2C, along with the development of NSCLC, the miR-196a expression was gradually increased. In comparison with the miR-196a expression at the I/II stage, miR-196a expression at the III/IV stage was increased. The results suggested that a higher miR-196a expression was synonymous with a worse condition of NSCLC patients. Therefore, miR-196 might be a potential target for the diagnosis of NSCLC.

To further confirm whether miR-196a was upregulated in NSCLC, 5 NSCLC cell lines (A549, H460, H1975, H1650, and HCC827) as well as the normal bronchial epithelial cell line (HBECs) were selected for determination of miR-196a expression using RT-qPCR. As shown in Fig. 2D, the expression of miR-196a increased significantly in all NSCLC cell lines in comparison with the normal cell line HBECs.

Additionally, the NSCLC cells were cultured and enriched in low-adhesion globules, with the expression of miR-196a measured by RT-qPCR. As demonstrated in Fig. 2E, the expression of miR-196a was higher in the A549 NSCLC cell spheres compared to the adherent differentiated cells ($p < 0.001$).

Moreover, the $CD133^{+/-}$ and $CD44^{+/-}$ NSCLC cells were isolated from A549 cells by flow cytometry (Fig. 2F) with an underlying purpose of further verifying the miR-196a expression in NSCLC. The results demonstrated that the miR-196a expression in the NSCLC $CD133^{+}$ and $CD44^{+}$ cells was significantly higher than that in NSCLC CD133- and CD44- cells ($p < 0.001$) (Fig. 2G). The aforementioned results suggested upregulation of miR-196a in NSCLC tissues and cells.

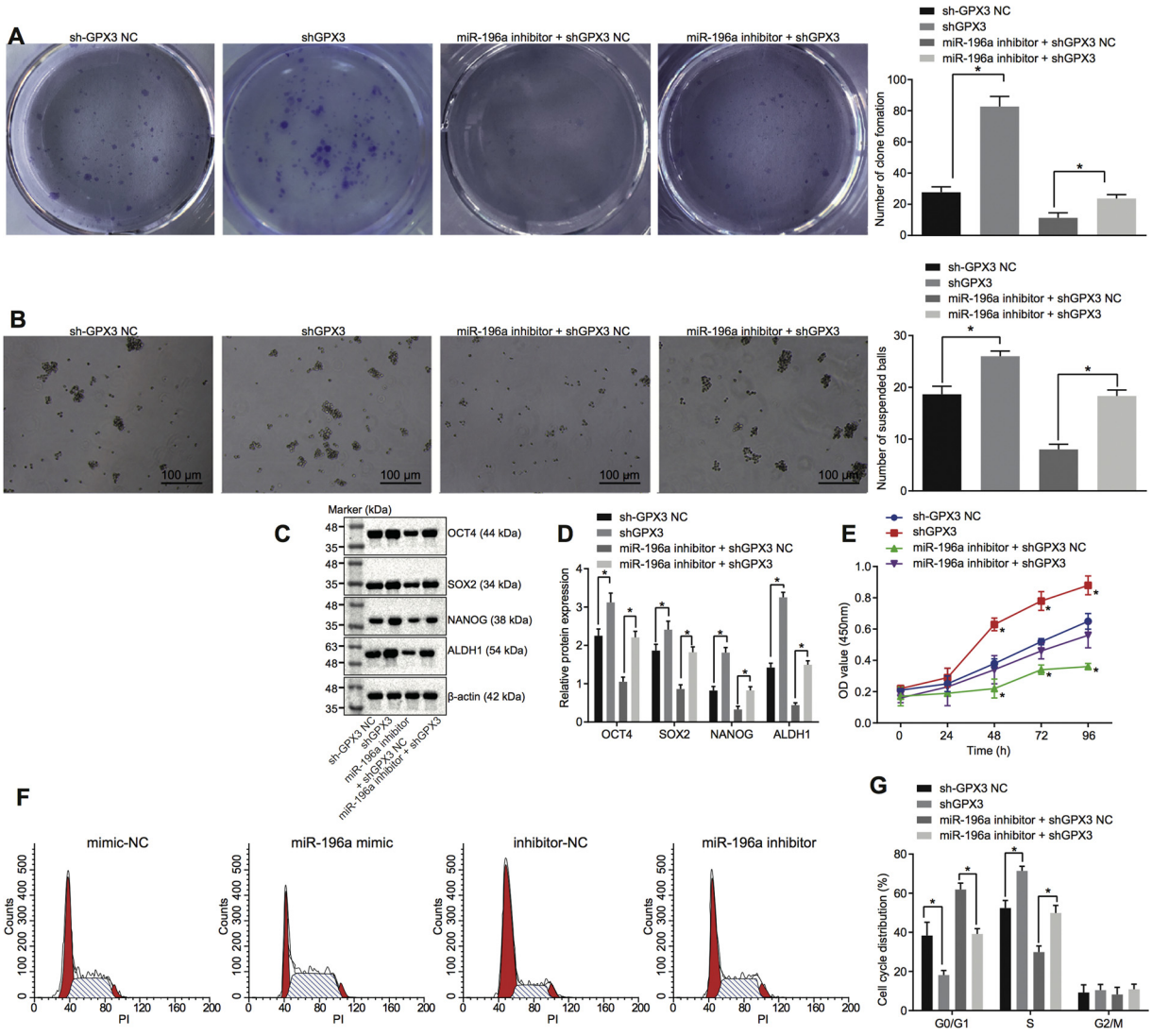

Fig. 6. Inhibition of miR-196a suppresses the NSCLC stem cell self-renewal ability and stemness by up-regulation of GPX3. A, cell colony formation ability of NSCLC cells after alteration of miR-196a and GPX3; B, cell sphere formation ability of NSCLC cells after alteration of miR-196a and GPX3 (× 100); C gray value of OCT4, SOX2, NANOG and ALDH1 protein bands after alteration of miR-196a and GPX3; D, relative protein levels of OCT4, SOX2, NANOG and ALDH1 in NSCLC cells after alteration of miR-196a and GPX3; E, proliferation of NSCLC stem cells after alteration of miR-196a detected by CCK-8 assay; F and G, cell cycle and distribution of NSCLC stem cells after alteration of miR-196a detected by flow cytometry. $^{*}p < 0.05$; the above data were measurement data and expressed as mean ± standard deviation; comparison among multiple groups was performed with one-way analysis of variance; the experiments were repeated 3 times; miR-196a, microRNA-196a; GPX3, glutathione peroxidase 3; ALDH1, aldehyde dehydrogenase 1; NSCLC, non-small-cell lung cancer; NC, negative control; SOX2, sex-determining region Y-box 2; OCT4, octamer-binding transcription factor 4.

3.3. Inhibition of miR-196a suppresses NSCLC stem cell self-renewal ability, stemness, viability and blocks cell cycle

CCK-8 assay, oncospheroids formation assay, colony formation assay and western blot analysis procedures were conducted to investigate the effect of miR-196a on A549 NSCLC stem cell viability, self-renewal ability and stemness after transfection with mimic-NC, miR-196a mimic, inhibitor-NC and miR-196a inhibitor. Cells transfected with the miR-196a mimic resulted in increased formed clone cell spheres and cell colonies (Fig. 3A and B), diameter and volume of clone cell spheres (Fig. 3B), *versus* transfection of mimic-NC. These results demonstrated that the NSCLC stem cell self-renewal ability and stemness enhanced by overexpressing miR-196a. In comparison with the treatment of inhibitor-NC, cells following transfection with miR-196a inhibitor showed decreased clone cell spheres and cell colonies (Fig. 3A and B), diameter and volume of clone cell spheres (Fig. 3B). Therefore, inhibition of miR-196a suppressed NSCLC stem cell self-renewal ability and stemness.

RT-qPCR was conducted to detect the transfection efficiency and the results showed that the miR-196a mimic increased miR-196a expression while the miR-196a inhibitor decreased miR-196a expression (Fig. 3C). Therefore, cells were transfected successfully and could be used for the further experimentation.

Western blot analysis showed that compared to the cells treated with miR-196a inhibitor NC, the cells treated with miR-196a inhibitor showed decreased protein expression of OCT4, SOX2, NANCG and ALDH ($p < 0.05$). In comparison to the cells treated with miR-196a mimic NC, the cells treated with miR-196a mimic showed increased protein expression of OCT4, SOX2, NANCG and ALDH ($p < 0.05$) (Fig. D and Fig. 3E).

CCK-8 assay showed that miR-196a mimic increased NSCLC cell viability while miR-196a inhibitor decreased NSCLC cell viability significantly ($p < 0.05$) (Fig. 3F).

PI single staining was conducted to detect the changes of cell cycle before and after transfection (Fig. 3G-H), and the results showed that compared to the cells treated with miR-196a mimic NC, cells treated

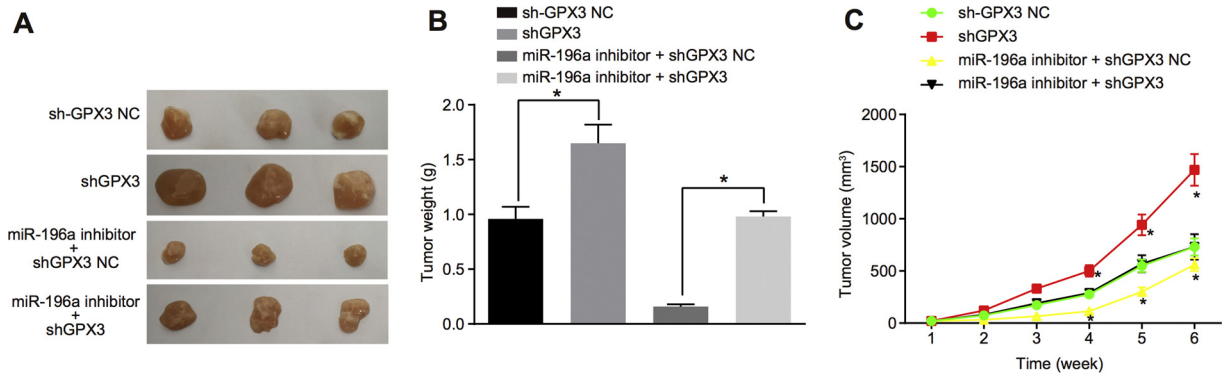

Fig. 7. Inhibition of miR-196a represses the tumor growth and tumorigenesis of NSCLC stem cells through activation of GPX3. A, the NSCLC tumor growth status in mice after alteration of miR-196a and GPX3; B, tumor weight in mice after alteration of miR-196a and GPX3; C, tumor volume at different time points after alteration of miR-196a and GPX3; $^{*}p < 0.05$; the above data were measurement data and expressed as mean ± standard deviation; comparison among multiple groups was performed with one-way analysis of variance; n = 7; miR-196a, microRNA-196a; GPX3, glutathione peroxidase 3; NSCLC, non-small-cell lung cancer; NC, negative control.

with miR-196a mimic showed decreased proportion of cells in the G0/G1 stage but increased proportion of cells in the S stage. In comparison with cells treated with miR-196a inhibitor NC, cells treated with miR-196 inhibitor showed an increased proportion of cells in the G0/G1 stage but a decreased proportion of cells in the S stage. Therefore, miR-196a mimic could promote cell cycle while miR-196a inhibitor could inhibit cell cycle.

3.4. Inhibition of miR-196a suppresses tumorigenicity in NSCLC stem cell

Xenograft tumor in nude mice was applied to study the effect of miR-196a on the tumorigenicity and tumor growth of A549 CSCs after transfection with mimic-NC, miR-196a mimic, inhibitor-NC, and miR-196a inhibitor. Reduced NSCLC tumor volume and weight were induced by treatment of miR-196a inhibitor, while increased tumor volume and weight were caused by treatment of miR-196a mimic (Fig. 4). Hence, NSCLC stem cell tumorigenicity in *vivo* was attenuated by repressing miR-196a.

3.5. miR-196a targets and negatively regulates GPX3

A bioinformatics prediction website TargetScan (http://www.targetscan.org/vert_72/) was adopted to predict the existence of a binding site between miR-196a and GPX3 (Fig. 5A), and target relationship between them was then further verified by dual-luciferase reporter gene assay. A 50% decline in luciferase activity was showed upon treatment with miR-196a mimic and WT-GPX3 ($p < 0.001$), while no significant difference in luciferase activity was observed upon treatment with miR-196a mimic and MUT-GPX3. In addition, no change in luciferase activity was shown upon treatment with the miR-196a inhibitor and inhibitor-NC ($p > 0.05$; Fig. 5B). Thus, it can be concluded that miR-196a could directly regulate GPX3.

Furthermore, western blot analysis was conducted to determine the expression of GPX3 in NSCLC tissues, and RT-qPCR was applied for the detection of miR-196a expression. According to the correlation analysis of NSCLC tissue samples acquired from the same patients, the expression of miR-196a was negatively correlated with the expression of GPX3 (Fig. 5C). The mRNA and protein expression of GPX3 was significantly decreased following treatment with miR-196a mimic ($p < 0.05$), while increased following treatment with miR-196a inhibitor ($p < 0.05$) (Fig. 5D and 5E). Taken together, miR-196a could target and inhibit expression of GPX3.

3.6. Inhibition of miR-196a hinders NSCLC stem cell stemness by upregulating GPX3

Oncospheroids formation assay and colony formation assay were applied to study the influence of miR-196a on the self-renewal ability and stemness of NSCLC stem cells isolated from A549 cells following a single treatment with either miR-196a inhibitor or GPX3 shRNA. As suggested in Fig. 6A–D, when compared with the treatment of sh-GPX3 NC, the abilities of colony formation and sphere formation as well as the protein levels of OCT4, SOX2, NANOG, and ALDH1 increased after delivery of sh-GPX3 ($p < 0.05$). After the delivery of both miR-196a inhibitor and sh-GPX3, the CSC abilities of colony formation and sphere formation as well as the protein levels of OCT4, SOX2, NANOG, and ALDH1 enhanced compared to delivery of both miR-196a inhibitor and sh-GPX3 NC ($p < 0.05$). Inactivation of GPX3 could reverse miR-196a inhibition-mediated suppressed NSCLC stem cell abilities of colony formation and sphere formation as well as the decreased protein levels of OCT4, SOX2, NANOG, and ALDH1.

Simultaneously, CCK-8 assay and PI single staining were performed to detect the proliferation and cell cycle, and the results showed that compared with the treatment of, the treatment of sh-GPX3 NC sh-GPX3 showed increased proliferation, decreased proportion of CSC at the G0/G1 stage and increased proportion of CSC at the S stage. Inactivation of GPX3 could reverse miR-196a inhibition-mediated decreased NSCLC stem cell proliferation and cell cycle (Fig. 6E-G). Collectively, inhibition of miR-196a repressed NSCLC stem cell stemness by up-regulation of GPX3.

3.7. Inhibition of miR-196a suppresses tumor growth via restoration of GPX3

Xenograft tumor in nude mice was conducted to investigate the effect of miR-196a-mediated GPX3 on tumorigenicity and tumor growth of NSCLC stem cells isolated from A549 cells following co-treatment with miR-196a inhibitor and GPX3 shRNA. The treatment of sh-GPX3 resulted in increased tumor volume and weight compared to treatment with sh-GPX3 NC, and the co-treatment of miR-196a inhibitor and sh-GPX3 also resulted in a synergistic effect compared to co-treatment with miR-196a inhibitor and sh-GPX3 NC ($p < 0.05$; Fig. 7). Hence, inhibition of miR-196a hindered NSCLC stem cell tumorigenicity in *vivo* by up-regulation of GPX3.

3.8. miR-196a induces activation of JNK pathway by silencing GPX3

To explore the interaction among miR-196a, GPX3 and JNK pathway, western blot analysis was conducted to determine the protein

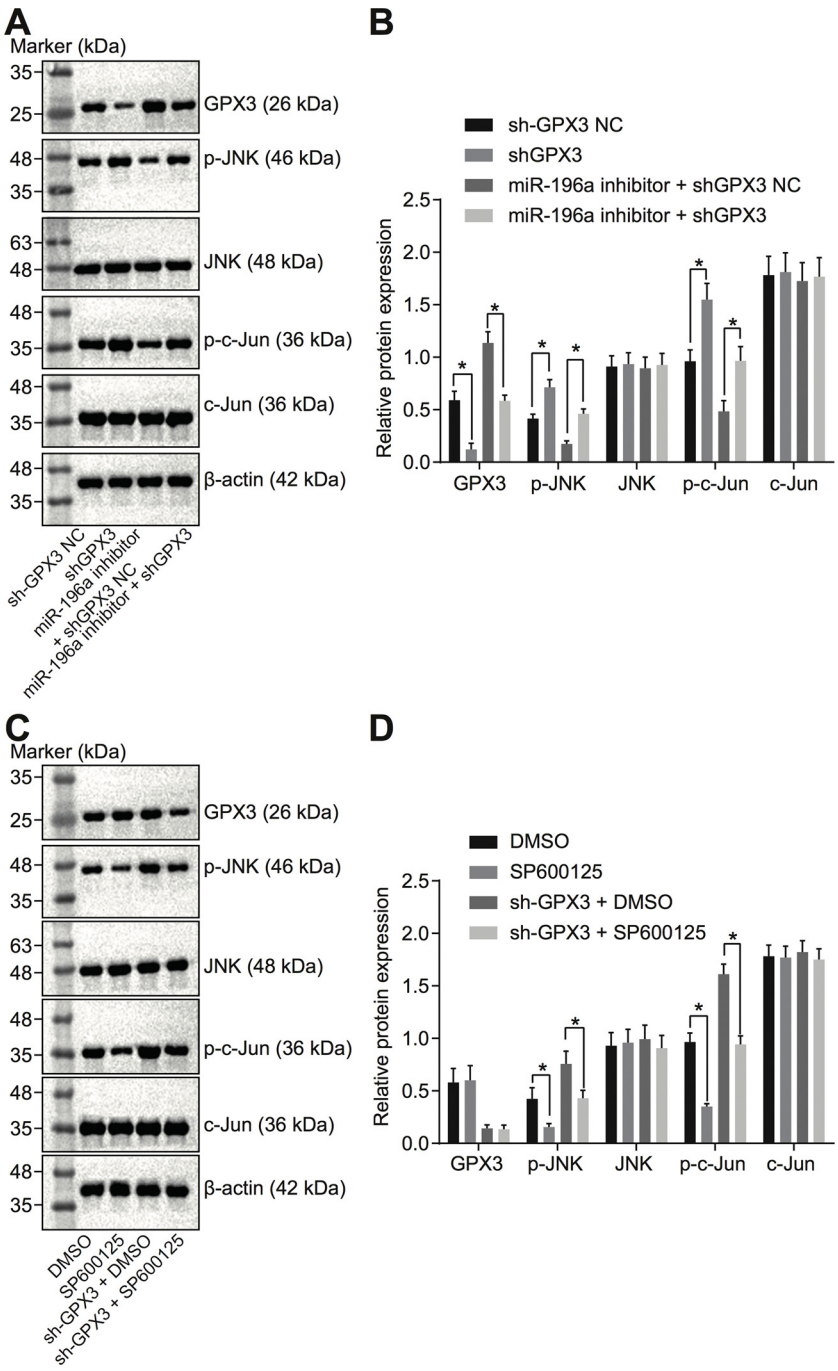

Fig. 8. miR-196a activates JNK pathway by silencing GPX3. A, gray value of GPX3, JNK, p-JNK, c-Jun, and p-c-Jun protein bands in NSCLC cells after alteration of miR-196a and GPX3; B, relative protein levels of GPX3, JNK, p-JNK, c-Jun, and p-c-Jun in NSCLC cells transfected with miR-196a inhibitor or sh-GPX3; C, gray value of GPX3, JNK, p-JNK, c-Jun, and p-c-Jun protein bands in NSCLC cells treated with sh-GPX3 or SP600125; D, protein levels of GPX3, JNK, p-JNK, c-Jun, and p-c-Jun in NSCLC cells transfected with sh-GPX3 or treated with SP600125; $^{*}p < 0.05$; the above data were measurement data, expressed as mean ± standard deviation, and compared with one-way analysis of variance; the experiments were repeated 3 times; miR-196a, microRNA-196a; GPX3, glutathione peroxidase 3; NSCLC, non-small-cell lung cancer; JNK, c-Jun NH-terminal kinase; NC, negative control.

levels of GPX3, JNK, and JNK pathway-related kinase (c-Jun) as well as the extent of JNK and c-Jun phosphorylation after a single treatment with either miR-196a inhibitor or GPX3 shRNA. Cells transfected with sh-GPX3 lead to decreased protein level of GPX3, increased extent of JNK and c-Jun phosphorylation, and unaffected protein levels of JNK and c-Jun compared to the cells transfected with sh-GPX3 NC; while cells co-transfected with miR-196a inhibitor and sh-GPX3 exhibited a lower protein level of GPX3, elevated extent of JNK and c-Jun phosphorylation, and still constant protein levels of JNK and c-Jun in comparison with the cells co-transfected with miR-196a inhibitor and sh-GPX3 NC ($p < 0.05$; Fig. 8A and B).

Furthermore, the protein levels of GPX3, JNK, c-Jun and the extent of JNK and c-Jun phosphorylation were assessed again after treatment of the JNK pathway inhibitor (SP600125). As demonstrated in Fig. 8C and 8D, CSCs delivering SP600125 exhibited unchanged protein levels of GPX3, JNK and c-Jun yet inhibited the extent of JNK and c-Jun phosphorylation, while CSCs co-treated with sh-GPX3 and SP600125 displayed unchanged GPX3, JNK, and c-Jun protein levels, and reduced the extent of JNK and c-Jun phosphorylation compared with CSCs co-treated with sh-GPX3 and DMSO. Thereby, miR-196a could activate the JNK pathway through downregulation of GPX3.

3.9. Inhibition of miR-196a upregulates E-cadherin and downregulates N-cadherin

RT-qPCR and western blot analysis were conducted to detect the effect of miR-196a on the metastasis and invasion of CSCs. In comparison to the treatment of miR-196a mimic NC, the treatment of miR-196a mimic inhibited mRNA and protein expression of E-cadherin and promoted the mRNA and protein expression of N-cadherin. Conversely,

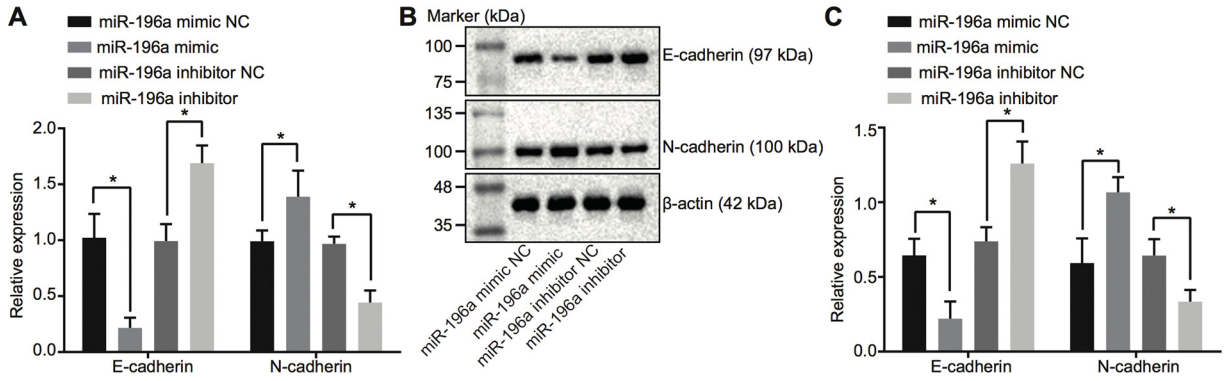

Fig. 9. Inhibition of miR-196a inhibits metastasis and invasion of the NSCLC stem cells. A, mRNA expression of E-cadherin and N-cadherin after treatment of NSCLC stem cells detected by RT-qPCR; B and C, protein expression of E-cadherin and N-cadherin after treatment of NSCLC stem cells detected by western blot analysis. $^{*}p < 0.05$; the above data were measurement data, expressed as mean ± standard deviation, and data between two groups were compared using independent sample *t*-test, multiple groups were compared using one-way analysis of variance; the experiments were repeated 3 times; miR-196a, microRNA-196a; GPX3, glutathione peroxidase 3; NSCLC, non-small-cell lung cancer; NC, negative control.

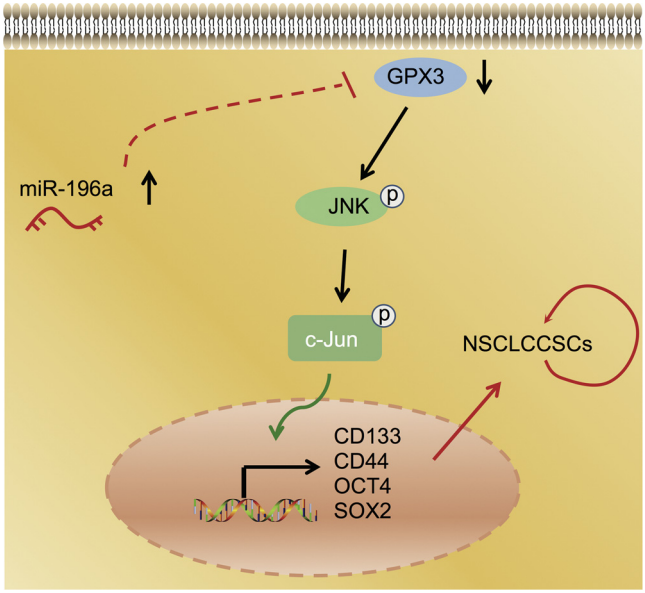

Fig. 10. Mechanism diagram underlies the regulatory role of miR-196a in NSCLC. miR-196a activated the JNK pathway through downregulation of GPX3, thus stimulating the protein levels of CD133, CD44, OCT4, SOX2 and promoting NSCLC stem cell self-renewal ability and stemness as a result. miR-196a, microRNA-196a; GPX3, glutathione peroxidase 3; JNK, Jun NH-terminal kinase; NSCLC, non-small-cell lung cancer; SOX2, sex-determining region Y-box 2; OCT4, octamer-binding transcription factor 4.

compared with the treatment of miR-196a inhibitor NC, the treatment of miR-196a inhibitor increased the mRNA and protein expression of E-cadherin and subsequently decreased the mRNA and protein expression of N-cadherin (Fig. 9). With these results, it can be speculated that miR-196a could promote CSC metastasis and invasion, while inhibition of miR-196a could inhibit CSC metastasis and invasion in NSCLC.

4. Discussion

Recent literature has suggested the functionality of various gene mutations as novel indicators of acquired resistance to therapy in NSCLC, yet the function of CSCs is unknown (Del Re et al., 2018). Several miRs are of significant importance in regulating the biological functions of CSCs (Liu and Tang, 2011). Our study aimed at investigating the role of miR-196a in the development of NSCLC stem cells. Collectively, data obtained from the present study revealed that miR-196a inhibition attenuated NSCLC stem cell self-renewal ability and stemness through inactivation of the GPX3-mediated JNK pathway.

The first intriguing finding of our study was that GPX3 is expressed at a poor level while miR-196a at a high level in NSCLC. miR-196a, whose upregulation persistently predicted unsatisfactory prognosis, typically functioned as an oncogene in various human cancers including ovarian cancer, osteosarcomas, and colorectal cancer (Ge et al., 2014; Zhang et al., 2014; Fan et al., 2015). Additionally, an increased expression of miR-196a has been observed in NSCLC cells, the downregulation of which had a suppressive effect on cell migration and invasion, but enhanced sensitivity to cisplatin therapy through apoptosis induction (Liu et al., 2012; Li et al., 2016). An existing study has reported that patients with lung cancer exhibited significantly reduced serum GPX3 levels, thereby speculating the prognostic value of GPX3 in patients in an operable stage (Oh et al., 2014). In regard to head and neck cancer, the loss of GPX3 expression resulting from promoter hypermethylation was suggested to function as a novel therapeutic target (Chen et al., 2011). Thus, the aforementioned evidence established a significant correlation between downregulated GPX3 and upregulated miR-196a with NSCLC progression.

According to dual luciferase reporter gene assay, GPX3 was a target gene of miR-196a. Besides, miR-196a overexpression or GPX3 downregulation activated the JNK pathway through elevating the extent of JNK and c-Jun phosphorylation. A report flagged the ability of miR-196a to facilitate esophageal cancer cell proliferation and inhibit apoptosis through negative regulation of annexin A1 (Luthra et al., 2008). Additionally, miR-196 was reported to regulate NSCLC cell proliferation and invasion through targeting the homeobox protein 5 (Liu et al., 2012). JNK is essential for the human glioma stem cell self-renewal ability and tumor formation, and might be linked to the maintenance of CSCs (Kitanaka et al., 2013). Inhibition of JNK signaling was illustrated to attenuate the self-renewal and tumor-initiating abilities of ovarian CSCs (Seino et al., 2014). Moreover, gonadotropin-releasing hormone was previously demonstrated to enhance stemness maintenance and the self-renewal capacity of lung cancer stem-like cells *via* activation of the JNK pathway (Lu et al., 2015). Moreover, activation of the JNK pathway was also suggested to be involved in NSCLC cell proliferation and invasion induced by Diversin (Luan et al., 2014). GPX3 was capable of inhibiting the JNK-c-Jun-Matrix metalloproteinase 2 pathway, thus exerting its suppressive effect on the tumor invasive behavior suppression in hepatocellular carcinoma (Qi et al., 2016). The aforementioned results evidently demonstrated the potential of miR-196a to activate the JNK pathway by down-regulating GPX3.

The last significant finding of our study was that inhibited expression of miR-196a and overexpressed GPX3 contributed to suppressive NSCLC stem cell self-renewal ability, stemness, tumorigenicity and

tumor growth by downregulating the levels of CSC-related markers (OCT4, SOX2, NANOG, and ALDH1). Stem cells are highly tumorigenic cancer cells exhibiting the ability of self-renewal and to differentiate into various cell types (Ogawa et al., 2017). NANOG is identified as a homeobox binding protein in embryonic stem cells, which is vital for regulating differentiation and self-renewal of embryonal stem cells and pluripotency during early embryonic stages (Freitag et al., 2017). SOX2 functions as a vital oncogene for organs with amplification of SOX2 locus at 3q26 and squamous cell carcinomas arising during lung cancer (Xiao et al., 2017). OCT4 has been shown to be a participant of maintaining CSC properties, and OCT4-upregulating NSCLC PC9 cells are demonstrative of a highly tumorigenic potential and a distinctively caused gefitinib resistance (Kobayashi et al., 2016). According to a recent study, there are an abundant of CSC-like properties in A459/CDDP cells with overexpressed CD133, CD44, SOX2, NANOG and OCT4 in NSCLC (Jiang et al., 2018), which are consistent with the current study. Moreover, miR-410 was documented to increase the levels of SOX2, OCT4, NANOG and C-X-C chemokine receptor type 4 and might induce the stemness of NSCLC stem cell *via* the miR-410/Glycogen synthase kinase 3β/β-catenin signaling axis (Ke et al., 2017). An aforementioned study suggested that normal hematopoietic stem cells overexpressing GPX3 were more competitive (Herault et al., 2012). Moreover, GPX3 was indicated to function as a tumor suppressor in lung cancer, and exert a suppressive effect on cell proliferation, migration and invasion *via* regulation of the redox-mediated signals (An et al., 2018). Collectively, the aforementioned findings supported the conclusion that miR-196a inhibition repressed NSCLC stem cell self-renewal ability, stemness, tumor growth and tumorigenicity through upregulation of GPX3.

To conclude, the key findings of this study revealed that inhibition of miR-196a could decrease NSCLC stem cell self-renewal ability, stemness, tumor growth and tumorigenicity through inactivation of the JNK pathway by upregulating GPX3 (Fig. 10). These findings may provide an insight aiding in a better approach for the treatment of NSCLC. It has been shown that miR-196a directly binds to the 3′ untranslated region of HOXA5, and *via* the down-regulation of HOXA5 to regulate NSCLC cell proliferation, migration and invasion (Liu et al., 2012). Due to limitations of time and energy, the relationship between HOXA5 and GPX3 was not fully detected. Therefore, further research should be conducted to detect the relationship between HOXA5 and GPX3 and to ascertain whether there is a possibility that miR-196a regulated HOXA5 and GPX3.

Declaration of Competing Interest

None.

Acknowledgements

This study was supported by Jiangxi Provincial Health Department Project (No. 20113032). We acknowledge and appreciate our colleagues for their valuable efforts and comments on this paper.

References

An, B.C., Choi, Y.D., Oh, I.J., Kim, J.H., Park, J.I., Lee, S.W., 2018. GPx3-mediated redox signaling arrests the cell cycle and acts as a tumor suppressor in lung cancer cell lines. PLoS One 13, e0204170.

An, B.C., Jung, N.K., Park, C.Y., Oh, I.J., Choi, Y.D., Park, J.I., Lee, S.W., 2016. Epigenetic and glucocorticoid receptor-mediated regulation of glutathione peroxidase 3 in lung Cancer cells. Mol. Cells 39, 631–638.

Apopa, P.L., Alley, L., Penney, R.B., Arnaoutakis, K., Steliga, M.A., Jeffus, S., Bircan, E., Gopalan, B., Jin, J., Patumcharoenpol, P., Jenjaroenpun, P., Wongsurawat, T., Shah, N., Boysen, G., Ussery, D., Nookaew, I., Fagan, P., Bebek, G., Orloff, M.S., 2018. PARP1 is up-regulated in non-small cell lung Cancer tissues in the presence of the cyanobacterial toxin microcystin. Front. Microbiol. 9, 1757.

Avisetti, D.R., Babu, K.S., Kalivendi, S.V., 2014. Activation of p38/JNK pathway is responsible for embelin induced apoptosis in lung cancer cells: transitional role of reactive oxygen species. PLoS One 9, e87050.

Cao, S., Wang, Z., Gao, X., He, W., Cai, Y., Chen, H., Xu, R., 2018. FOXC1 induces cancer stem cell-like properties through upregulation of beta-catenin in NSCLC. J. Exp. Clin. Cancer Res. 37, 220.

Chen, B., Rao, X., House, M.G., Nephew, K.P., Cullen, K.J., Guo, Z., 2011. GPx3 promoter hypermethylation is a frequent event in human cancer and is associated with tumorigenesis and chemotherapy response. Cancer Lett. 309, 37–45.

Del Re, M., Arrigoni, E., Restante, G., Passaro, A., Rofi, E., Crucitta, S., De Marinis, F., Di Paolo, A., Danesi, R., 2018. Concise Review: Resistance to Tyrosine Kinase Inhibitors in Non-Small Cell Lung Cancer: The Role of Cancer Stem Cells. Stem Cells 36, 633–640.

Fan, Y., Fan, J., Huang, L., Ye, M., Huang, Z., Wang, Y., Li, Q., Huang, J., 2015. Increased expression of microRNA-196a predicts poor prognosis in human ovarian carcinoma. Int. J. Clin. Exp. Pathol. 8, 4132–4137.

Freitag, D., McLean, A.L., Simon, M., Koch, A., Grube, S., Walter, J., Kalff, R., Ewald, C., 2017. NANOG overexpression and its correlation with stem cell and differentiation markers in meningiomas of different WHO grades. Mol. Carcinog. 56, 1953–1964.

Gautier, L., Cope, L., Bolstad, B.M., 2004. Irizarry RA. affy–analysis of Affymetrix GeneChip data at the probe level. Bioinformatics. 20, 307–315.

Ge, J., Chen, Z., Li, R., Lu, T., Xiao, G., 2014. Upregulation of microRNA-196a and microRNA-196b cooperatively correlate with aggressive progression and unfavorable prognosis in patients with colorectal cancer. Cancer Cell Int. 14, 128.

Guerriero, I., D'Angelo, D., Pallante, P., Santos, M., Scrima, M., Malanga, D., De Marco, C., Ravo, M., Weisz, A., Laudanna, C., Ceccarelli, M., Falco, G., Rizzuto, A., Viglietto, G., 2017. Analysis of miRNA profiles identified miR-196a as a crucial mediator of aberrant PI3K/AKT signaling in lung cancer cells. Oncotarget. 8, 19172–19191.

Halim, N.H.A., Zakaria, N., Satar, N.A., Yahaya, B.H., 2016. Isolation and characterization of Cancer stem cells of the non-small-Cell lung Cancer (A549) cell line. Methods Mol. Biol. 1516, 371–388.

Herault, O., Hope, K.J., Deneault, E., Mayotte, N., Chagraoui, J., Wilhelm, B.T., Cellot, S., Sauvageau, M., Andrade-Navarro, M.A., Hebert, J., Sauvageau, G., 2012. A role for GPx3 in activity of normal and leukemia stem cells. J. Exp. Med. 209, 895–901.

Jiang, P., Xu, C., Chen, L., Chen, A., Wu, X., Zhou, M., Haq, I.U., Mariyam, Z., Feng, Q., 2018. EGCG inhibits CSC-like properties through targeting miR-485/CD44 axis in A549-cisplatin resistant cells. Mol. Carcinog. 57, 1835–1844.

Jin, B., Jin, H., Wu, H.B., Xu, J.J., Li, B., 2018. Long non-coding RNA SNHG15 promotes CDK14 expression via miR-486 to accelerate non-small cell lung cancer cells progression and metastasis. J. Cell. Physiol. 233, 7164–7172.

Ke, X., Yuan, Y., Guo, C., Yang, Y., Pu, Q., Hu, X., Tang, K., Luo, X., Jiang, Q., Su, X., Liu, L., Zhu, W., Wei, Y., 2017. MiR-410 induces stemness by inhibiting Gsk3beta but upregulating beta-catenin in non-small cells lung cancer. Oncotarget. 8, 11356–11371.

Kim, J., So, S., Lee, H.J., Park, J.C., Kim, J.J., Lee, H., 2013. DigSee: disease gene search engine with evidence sentences (version cancer). Nucleic Acids Res. 41, W510–517.

Kitanaka, C., Sato, A., Okada, M., 2013. JNK signaling in the control of the tumor-initiating capacity associated with Cancer stem cells. Genes Cancer 4, 388–396.

Kobayashi, I., Takahashi, F., Nurwidya, F., Nara, T., Hashimoto, M., Murakami, A., Yagishita, S., Tajima, K., Hidayat, M., Shimada, N., Suina, K., Yoshioka, Y., Sasaki, S., Moriyama, M., Moriyama, H., Takahashi, K., 2016. Oct4 plays a crucial role in the maintenance of gefitinib-resistant lung cancer stem cells. Biochem. Biophys. Res. Commun. 473, 125–132.

Li, Q., Yang, Z., Chen, M., Liu, Y., 2016. Downregulation of microRNA-196a enhances the sensitivity of non-small cell lung cancer cells to cisplatin treatment. Int. J. Mol. Med. 37, 1067–1074.

Liu, C., Tang, D.G., 2011. MicroRNA regulation of cancer stem cells. Cancer Res. 71, 5950–5954.

Liu, K., Jin, M., Xiao, L., Liu, H., Wei, S., 2018. Distinct prognostic values of mRNA expression of glutathione peroxidases in non-small cell lung cancer. Cancer Manag. Res. 10, 2997–3005.

Liu, X.H., Lu, K.H., Wang, K.M., Sun, M., Zhang, E.B., Yang, J.S., Yin, D.D., Liu, Z.L., Zhou, J., Liu, Z.J., De, W., Wang, Z.X., 2012. MicroRNA-196a promotes non-small cell lung cancer cell proliferation and invasion through targeting HOXA5. BMC Cancer 12, 348.

Lu, C., Huang, T., Chen, W., Lu, H., 2015. GnRH participates in the self-renewal of A549-derived lung cancer stem-like cells through upregulation of the JNK signaling pathway. Oncol. Rep. 34, 244–250.

Lu, Y.C., Chang, J.T., Liao, C.T., Kang, C.J., Huang, S.F., Chen, I.H., Huang, C.C., Huang, Y.C., Chen, W.H., Tsai, C.Y., Wang, H.M., Yen, T.C., You, G.R., Chiang, C.H., Cheng, A.J., 2014. OncomiR-196 promotes an invasive phenotype in oral cancer through the NME4-JNK-TIMP1-MMP signaling pathway. Mol. Cancer 13, 218.

Luan, L., Zhao, Y., Xu, Z., Jiang, G., Zhang, X., Fan, C., Liu, D., Zhao, H., Xu, K., Wang, M., Yu, X., Wang, E., 2014. Diversin increases the proliferation and invasion ability of non-small-cell lung cancer cells via JNK pathway. Cancer Lett. 344, 232–238.

Luthra, R., Singh, R.R., Luthra, M.G., Li, Y.X., Hannah, C., Romans, A.M., Barkoh, B.A., Chen, S.S., Ensor, J., Maru, D.M., Broaddus, R.R., Rashid, A., Albarracin, C.T., 2008. MicroRNA-196a targets annexin A1: a microRNA-mediated mechanism of annexin A1 downregulation in cancers. Oncogene. 27, 6667–6678.

Mauguen, A., Pignon, J.P., Burdett, S., Domerg, C., Fisher, D., Paulus, R., Mandrekar, S.J., Belani, C.P., Shepherd, F.A., Eisen, T., Pang, H., Collette, L., Sause, W.T., Dahlberg, S.E., Crawford, J., O'Brien, M., Schild, S.E., Parmar, M., Tierney, J.F., Le Pechoux, C., Michiels, S., Surrogate Lung Project Collaborative G, 2013. Surrogate endpoints for overall survival in chemotherapy and radiotherapy trials in operable and locally advanced lung cancer: a re-analysis of meta-analyses of individual patients' data. Lancet Oncol. 14, 619–626.

Ogawa, T., Hirohashi, Y., Murai, A., Nishidate, T., Okita, K., Wang, L., Ikehara, Y., Satoyoshi, T., Usui, A., Kubo, T., Nakastugawa, M., Kanaseki, T., Tsukahara, T., Kutomi, G., Furuhata, T., Hirata, K., Sato, N., Mizuguchi, T., Takemasa, I., Torigoe, T.,

2017. ST6GALNAC1 plays important roles in enhancing cancer stem phenotypes of colorectal cancer via the Akt pathway. Oncotarget. 8, 112550–112564.
Oh, I.J., Kim, H.E., Song, S.Y., Na, K.J., Kim, K.S., Kim, Y.C., Lee, S.W., 2014. Diagnostic value of serum glutathione peroxidase 3 levels in patients with lung cancer. Thorac. Cancer 5, 425–430.
Qi, X., Ng, K.T., Shao, Y., Li, C.X., Geng, W., Ling, C.C., Ma, Y.Y., Liu, X.B., Liu, H., Liu, J., Yeung, W.H., Lo, C.M., Man, K., 2016. The clinical significance and potential therapeutic role of GPx3 in tumor recurrence after liver transplantation. Theranostics. 6, 1934–1946.
Seino, M., Okada, M., Shibuya, K., Seino, S., Suzuki, S., Ohta, T., Kurachi, H., Kitanaka, C., 2014. Requirement of JNK signaling for self-renewal and tumor-initiating capacity of ovarian cancer stem cells. Anticancer Res. 34, 4723–4731.
Shannon, P., Markiel, A., Ozier, O., Baliga, N.S., Wang, J.T., Ramage, D., Amin, N., Schwikowski, B., Ideker, T., 2003. Cytoscape: a software environment for integrated models of biomolecular interaction networks. Genome Res. 13, 2498–2504.
Smyth, G.K., 2004. Linear models and empirical bayes methods for assessing differential expression in microarray experiments. Stat. Appl. Genet. Mol. Biol. 3 Article3.
Song, W., Ma, Y., Wang, J., Brantley-Sieders, D., Chen, J., 2014. JNK signaling mediates EPHA2-dependent tumor cell proliferation, motility, and cancer stem cell-like properties in non-small cell lung cancer. Cancer Res. 74, 2444–2454.
Szklarczyk, D., Franceschini, A., Wyder, S., Forslund, K., Heller, D., Huerta-Cepas, J., Simonovic, M., Roth, A., Santos, A., Tsafou, K.P., Kuhn, M., Bork, P., Jensen, L.J., von Mering, C., 2015. STRING v10: protein-protein interaction networks, integrated over the tree of life. Nucleic Acids Res. 43, D447–452.
Xiao, Z.J., Liu, J., Wang, S.Q., Zhu, Y., Gao, X.Y., Tin, V.P., Qin, J., Wang, J.W., Wong, M.P., 2017. NFATc2 enhances tumor-initiating phenotypes through the NFATc2/SOX2/ALDH axis in lung adenocarcinoma. Elife. 6.
Xu, L., Wei, B., Hui, H., Sun, Y., Liu, Y., Yu, X., Dai, J., 2018. Positive feedback loop of lncRNA LINC01296/miR-598/Twist1 promotes non-small cell lung cancer tumorigenesis. J. Cell. Physiol.
Yang, C.L., Zheng, X.L., Ye, K., Ge, H., Sun, Y.N., Lu, Y.F., Fan, Q.X., 2018. MicroRNA-183 acts as a tumor suppressor in human non-small cell lung Cancer by down-regulating MTA1. Cell. Physiol. Biochem. 46, 93–106.
Yin, H., Ma, J., Chen, L., Piao, S., Zhang, Y., Zhang, S., Ma, H., Li, Y., Qu, Y., Wang, X., Xu, Q., 2018. MiR-99a enhances the radiation sensitivity of non-small cell lung Cancer by targeting mTOR. Cell. Physiol. Biochem. 46, 471–481.
Zhang, C., Yao, C., Li, H., Wang, G., He, X., 2014. Combined elevation of microRNA-196a and microRNA-196b in sera predicts unfavorable prognosis in patients with osteosarcomas. Int. J. Mol. Sci. 15, 6544–6555.